



Comparisons of in situ measurements of cirrus cloud ice water content

Sean M. Davis,¹ Linnea M. Avallone,¹ Elliot M. Weinstock,² Cynthia H. Twohy,³
Jessica B. Smith,² and Gregory L. Kok⁴

Received 2 November 2006; revised 2 February 2007; accepted 5 February 2007; published 22 May 2007.

[1] Aircraft-based in situ measurements of cirrus cloud ice water content (IWC) are important for cloud microphysical/radiative modeling and satellite validation studies, yet the measurements have proven challenging due, in part, to the large dynamic range of IWC values present in cirrus clouds. To date, three instruments designed for the measurement of IWC have been flown aboard the NASA WB-57F research aircraft: the University of Colorado closed-path laser hygrometer, the Droplet Measurement Technologies Cloud Spectrometer and Impactor, and the Harvard University Lyman- α total water photofragment-fluorescence hygrometer. This paper compares IWC measurements from these three instruments taken during the Midlatitude Cirrus Experiment (MidCiX) in 2004. At larger values of IWC ($IWC > 10 \text{ mg m}^{-3}$), the three instruments agree, on average, to within 20%, which is of the order of their estimated instrumental uncertainties. At smaller IWC values ($< 10 \text{ mg m}^{-3}$), the agreement is worse, in part due to increasing instrument uncertainties. These results have implications for measurements in thin and subvisual cirrus. Particle sampling and evaporation, instrument background levels, and hysteresis are not found to be significant contributors to discrepancies among the measurements. For remote sensing validation studies where IWC data are vertically integrated to obtain ice water path, the agreement between the instruments is better than 20% for thick cirrus ($\tau > 1$), implying that IWC measurements in thicker clouds are of sufficient accuracy for validation studies.

Citation: Davis, S. M., L. M. Avallone, E. M. Weinstock, C. H. Twohy, J. B. Smith, and G. L. Kok (2007), Comparisons of in situ measurements of cirrus cloud ice water content, *J. Geophys. Res.*, 112, D10212, doi:10.1029/2006JD008214.

1. Introduction

[2] One of the greatest uncertainties in our current understanding of Earth's climate is the impact of clouds, in terms of both their radiative properties and their future role in mitigating or enhancing climate change. Within this context, cirrus clouds are particularly important because of their impact on radiative forcing and on stratospheric water vapor and ozone [Houghton *et al.*, 2001]. To a good approximation, ice water content (IWC), along with the effective radius, r_e , and asymmetry parameter, g , determines the optical depth (τ), albedo, and net radiative forcing of cirrus clouds. Depending on the specific combination of microphysical parameters, cirrus clouds may cause either a positive or a negative radiative forcing [Liou, 1986; Lohmann and Roeckner, 1995], and understanding the net global effect of cirrus clouds depends largely on the ability of satellite monitoring systems and general circula-

tion models (GCMs) to accurately retrieve and quantify cirrus cloud properties.

[3] In recent years, several satellite instruments have been launched specifically for the purpose of remotely sensing clouds, including cirrus clouds. Other existing satellite instruments exhibit sensitivity to cirrus clouds, and these sensitivities have been exploited to retrieve or infer ice cloud microphysical properties. As an example, the GOES satellites, originally launched for the purpose of weather observations, have been used to retrieve cirrus optical depth and ice water path [Minnis *et al.*, 1995], which is the integral of IWC over the vertical column ($IWP = \int_z IWC \, dz$). In addition, retrieval of cirrus microphysical properties are being made from several sensors aboard NASA satellite platforms, including AIRS aboard Aqua [Aumann *et al.*, 2003], MODIS aboard Terra and Aqua [Gao and Kaufman, 1995; King *et al.*, 1992], CALIOP on CALIPSO [Heymsfield *et al.*, 2005; Vaughan *et al.*, 2004], mm-wavelength radar aboard CloudSat [Stephens *et al.*, 2002], and MLS aboard Aura [Waters *et al.*, 2006]. From these instruments, IWC or IWP can either be directly retrieved, or inferred from other retrieved properties such as optical depth. Assumptions regarding ice crystal properties (for example, size, habit) are typically required for the retrieval forward models, in addition to other atmospheric state parameters. Thus sensitivity testing and validation of these retrievals will largely rely on data taken by ground-based radar and/or lidar

¹Laboratory for Atmospheric and Space Physics, University of Colorado, Boulder, Colorado, USA.

²Department of Chemistry and Chemical Biology, Harvard University, Cambridge, Massachusetts, USA.

³College of Oceanography and Atmospheric Sciences, Oregon State University, Corvallis, Oregon, USA.

⁴Droplet Measurement Technologies, Boulder, Colorado, USA.

and aircraft in situ measurements such as IWC or IWP. Verification of the accuracy of satellite IWC or IWP should rely on observations made by instruments with significantly better accuracy; in this case, presumably those provided by in situ sensors. However, to date, the accuracy of in situ measurements of cirrus IWC have not been established.

[4] In addition to improving satellite retrievals, in situ measurements of cirrus microphysics will aid in advancing model capabilities to predict climate change via improved parameterizations of cirrus cloud microphysics. Currently, many GCMs use IWC, or the related variable IWP, as a prognostic variable [Joseph and Wang, 1999; Kao and Smith, 1999; McFarquhar *et al.*, 2003] from which to obtain other radiatively important properties such as single-scattering albedo, optical depth, and infrared emissivity. Verifying and expanding upon these representations of cirrus clouds in global models will be facilitated through a synergy of ground-based, aircraft in situ, and space-based measurements.

[5] In situ measurements will also aid in resolving the discrepancy between the magnitude of the global upper tropospheric ice distribution observed in satellite data and that predicted by GCMs. Although there are similar spatial patterns in the distribution of upper tropospheric (UT) ice, there is still disagreement of a factor of about 2–3 between the global distribution of upper tropospheric ice measured by AURA MLS and that calculated by several GCMs [Li *et al.*, 2005].

[6] This paper addresses the overall accuracy of in situ measurements of cirrus IWC and their utility for comparisons with satellite data by comparing simultaneous observations from three instruments that use three different measurement techniques. In the next section of the paper, the instruments, data sets, and comparison methods are described. Then comparisons are made between observations from the various instruments, with consideration given to the stated instrumental uncertainties and differences in instrument and sampling characteristics. Some specific examples of cloud encounters are presented, and the implications of measurement differences are discussed with regard to satellite validation studies.

2. Instruments and Methods

[7] The cirrus IWC data sets analyzed in this paper come from two field campaigns, Cirrus Regional Study of Tropical Anvils and Cirrus Layers: Florida Area Cirrus Experiment (CRYSTAL-FACE) in 2002 and Midlatitude Cirrus Experiment (MidCiX) in 2004.

[8] During CRYSTAL-FACE, which was based out of Boca Chica Naval Air Field near Key West, Florida, six aircraft and two radar ground sites were used to profile tropical cirrus as well as large tropical convective systems and their associated anvil outflow [Jensen *et al.*, 2004]. Measurements of cirrus IWC discussed in this paper were made from the NASA WB-57F aircraft over 14 flights that totaled approximately 61 flight hours and included over 10 hours of in-cloud flight.

[9] Data were also obtained during the 2004 MidCiX mission that was based out of Ellington Field in Houston, Texas. The objective of this campaign was to sample a variety of midlatitude ice clouds from the NASA WB-57F

aircraft in conjunction with ground-based measurements at the DOE-ARM SGP site in north-central Oklahoma and coincident with satellite measurements from NASA Aqua and Terra platforms. MidCiX consisted of about 50 flight hours over nine flights, with ~20 hours of in-cloud flight. Clouds sampled during this mission ranged from cirrus clouds formed in situ to convectively generated cirrus to mountain wave clouds over the Rocky Mountains.

[10] During MidCiX, several instruments that measure bulk cirrus IWC flew aboard the NASA WB-57F. These instruments were the Cloud Spectrometer and Impactor (CSI) developed by Droplet Measurement Technologies and Oregon State University; the University of Colorado closed-path laser hygrometer (CLH); and the Harvard University Lyman- α total water photofragment-fluorescence hygrometer (HT).

[11] The CSI measures enhanced condensed water content after separating cloud droplets and ice crystals from interstitial water vapor using a counterflow virtual impactor [Twohy *et al.*, 1997]. The CSI uses a tunable diode laser hygrometer (Maycomm Instruments) to measure the water vapor remaining after water particles (liquid or solid) flowing through a heated inlet are evaporated. Particle sampling is subisokinetic with particle enhancements of about a factor of 25–50 depending on flow rate settings for a particular flight. The inlet has an aerodynamic cut diameter (defined as the minimum particle size collected with 50% efficiency) that varies with air speed and pressure. The cut size was about 5 μm for typical MidCiX flight conditions. Enhanced IWC is measured at a sample rate of 1 Hz by the CSI. During CRYSTAL-FACE, a Lyman- α hygrometer attached to the CVI [Twohy *et al.*, 1997] flew aboard a different aircraft than the WB-57F, so no CSI data from CRYSTAL-FACE is discussed in this paper.

[12] The Harvard Lyman- α total water photofragment-fluorescence hygrometer (HT) measures “total water” (condensed plus vapor) [Weinstock *et al.*, 2006a]. Water vapor, measured simultaneously by the Harvard water vapor instrument [Weinstock *et al.*, 1994], is subtracted to determine condensed water content. The HT inlet is attached to a pump to maintain isokinetic particle sampling. Particles flowing through the inlet are evaporated, and the resulting water vapor is measured by a Lyman- α photofragment fluorescence technique. In this technique, a 121.6-nm (Lyman- α) lamp photodissociates water vapor, and the resulting fluorescence from OH is detected by a photomultiplier tube set at right angles to the lamp. The Harvard Lyman- α instruments take data at 10 Hz, which are averaged to 0.1 or 1 Hz to achieve a desired signal-to-noise level. Data were archived at 0.1 Hz during CRYSTAL-FACE and at 1 Hz during MidCiX. During CRYSTAL-FACE, scattered light signals in the Harvard total water instrument indicated the presence of incompletely evaporated particles. Because of this, a 50- μm stainless-steel mesh screen was inserted between sections of the inlet heater after CRYSTAL FACE to facilitate the evaporation of large ice particles [Weinstock *et al.*, 2006b].

[13] The University of Colorado closed-path tunable diode laser hygrometer (CLH) is a total water instrument that was coupled to a subisokinetic inlet aboard the WB-57F aircraft during the CRYSTAL-FACE and MidCiX campaigns. The CLH uses second harmonic (2f) infrared spectroscopy for the detection of water vapor resulting from

the evaporation of cloud particles in a heated inlet [Davis *et al.*, 2007]. Particles are enhanced relative to their ambient concentrations by factors of between 40 and 60, depending on aircraft speed and flow speed through the instrument, which is determined by a mass flow controller. Particle sampling efficiency is a function of particle size, ranging from $\sim 5\%$ for particles $1\ \mu\text{m}$ in diameter to 90% for $30\ \mu\text{m}$ diameter particles, and asymptoting to 100% . Details of the CLH inlet, particle sampling, calibration, and IWC determination are provided by Davis *et al.* [2007]. IWC is calculated every $1.5\ \text{s}$ ($0.66\ \text{Hz}$) from the CLH enhanced total water (eTW) measurement after subtracting water vapor obtained from either the Harvard Lyman- α [Weinstock *et al.*, 1994] or JPL laser hygrometer [May, 1998], removing a background offset [Hallar *et al.*, 2004], and dividing by a particle enhancement factor. Particle enhancement is calculated using data from the WB-57F meteorological measurement system [Scott *et al.*, 1990] and (when available) particle size distributions from the cloud and aerosol precipitation spectrometer [Baumgardner *et al.*, 2001].

[14] During both missions described in this paper, the CLH was mounted on the right wing pod of the WB-57F aircraft with its inlet on the leading edge, and the HT instrument was mounted in the forwardmost pallet below the aircraft fuselage. During MidCiX, the CSI was mounted above the right wing pod of the WB-57F. Other than the insertion of the mesh screen in the HT instrument, the configurations and locations of the CLH and HT instruments on the WB-57F were identical for CRYSTAL-FACE and MidCiX.

[15] The estimated uncertainties in IWC for each instrument are given here. During MidCiX, the CSI uncertainty (1σ) is estimated at about 11% at water contents of 50 to $1000\ \text{mg m}^{-3}$, increasing to 15% at $5\ \text{mg m}^{-3}$, and to 23% at $2.5\ \text{mg m}^{-3}$ and smaller [Heymsfield *et al.*, 2006]. The components contributing to the CSI uncertainty are the water vapor measurement (5%), enhancement factor uncertainty (10%), and a clear-air baseline offset. The increase of the CSI uncertainty at low IWC is the result of sensor zero offset of less than $50\ \text{mg m}^{-3}$ ($2\ \text{mg m}^{-3}$ in IWC) that is pressure dependent. This offset is removed in the final processing by deriving a pressure-dependent fit to clear-air data.

[16] For CRYSTAL-FACE, the HT IWC uncertainty (1σ) was 18% [Weinstock *et al.*, 2006a] with contributions from particle sampling (15%), total water and water vapor measurements (5% each), hysteresis (5%), and ice crystal evaporation (5%). For MidCiX, the uncertainties are the same, except for the assumption that ice crystal evaporation does not contribute to the uncertainty. This yields a 1σ uncertainty of 17% in the TW measurement.

[17] Contributions to the CLH IWC uncertainty arise from the CLH water vapor measurement (5%), ambient water vapor (5%), and data used for calculating the enhancement factor: flow rate (10%), true air speed ($\sim 1\%$), the inlet enhancement curve (5%), and particle size distribution measurements (5%) [Davis *et al.*, 2007]. The uncertainty of each CLH IWC measurement is estimated using specific values of the factors outlined above, but the uncertainty is roughly a function of IWC (similar to that reported for the CSI). During CRYSTAL-FACE and MidCiX, the CLH

uncertainty (1σ) is approximately 11% at IWC values above $5\ \text{mg m}^{-3}$ and increases to about 50% at values at and below $1\ \text{mg m}^{-3}$ [Davis *et al.*, 2007].

[18] Because the three IWC data sets are taken at different frequencies and time-tagged differently, it is necessary to interpolate and shift the IWC data sets for each flight. In these comparisons, the CSI and HT data are stored at 1-s , and the CLH data are at 1.5-s . CSI and HT data are interpolated onto the timescale of the CLH data, and shifted such that the maximum cross-correlation between the measurements is achieved.

3. Mission-Level Comparisons

3.1. General Comparisons

[19] The broadest comparisons between the IWC measurements are shown in Figure 1 for the various pairings of instruments during MidCiX, and in Figure 2 for CLH and HT during CRYSTAL-FACE. In both of these figures, data from one instrument are plotted against data from another instrument, and the 1:1 line (dashed) and least squares fit line (solid) are shown. The comparisons and fits are shown on both linear and logarithmic scales to emphasize the large range of values over which IWC is measured. In addition, the percent difference between the instruments is shown as a function of absolute IWC. The data shown in Figures 1 and 2 are for time periods in which all three bulk IWC instruments simultaneously recorded $\text{IWC} > 1\ \text{mg m}^{-3}$, and both the CAPS and Cloud Particle Imager [Lawson and Jensen, 1998; Lawson *et al.*, 2001] instruments recorded particle counts. These strict criteria are cloudy-condition conservative, in that they eliminate a data point if any of the instruments indicate that the WB-57F is not in a cloud. These criteria were chosen to avoid including clear-air data from the instruments.

[20] During both CRYSTAL-FACE and MidCiX, the bulk IWC measurements are reasonably well correlated ($r^2 = 0.6$ for CRYSTAL-FACE, ~ 0.95 or greater for MidCiX) with one another. The slopes of the best fit lines are in the range of $0.8\text{--}1.0$, indicating agreement roughly to within 20% . Although the measurement conditions were different during each mission (i.e., CRYSTAL-FACE flights were typically at higher altitude, with lower ambient water vapor and larger IWC than MidCiX), the CLH is on average $10\text{--}20\%$ lower than HT over a broad range of IWC, as evidenced by the bottom row of plots in Figures 1 and 2. A similar behavior is present between the CSI and HT for MidCiX.

[21] One striking feature in the plots of percent difference versus IWC for the MidCiX campaign is the large differences at IWC values less than about $10\ \text{mg m}^{-3}$. Binned median values of CLH and CSI are around 25% lower than HT measurements, and CLH data are upwards of 20% larger than CSI at the smallest values (bottom row, Figure 1). One possible explanation for the differences present would be a small baseline offset in the HT IWC data. However, the Harvard total water and water vapor measurements typically agree to within $\pm 1\ \text{ppmv}$ ($\sim 0.1\ \text{mg m}^{-3}$) in clear air, so this explanation appears to fail. A complicating factor in identifying the cause of relatively larger HT values at small IWC is that the feature does not appear in the CRYSTAL-FACE data. The differences between CLH and

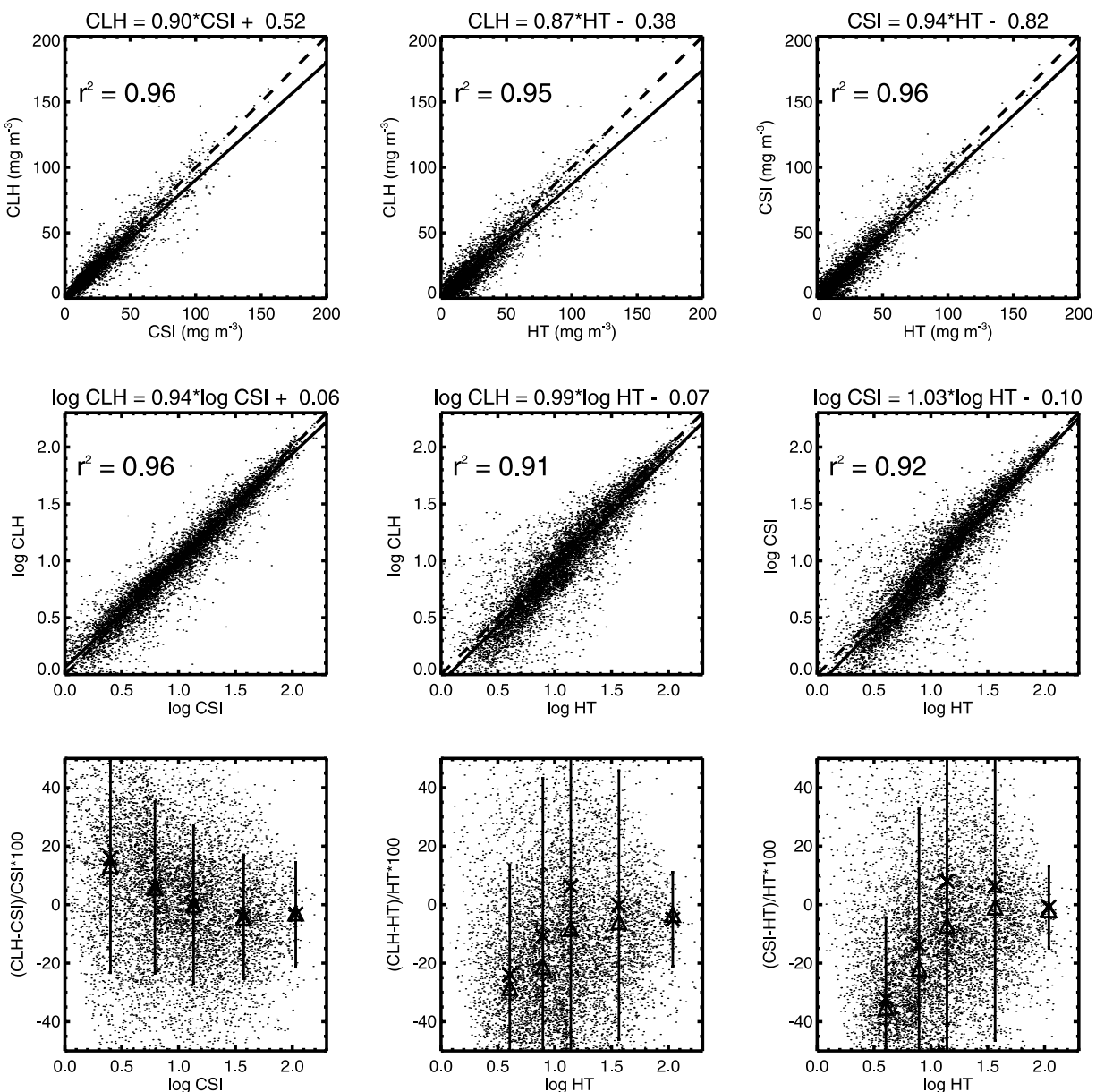


Figure 1. MidCiX IWC comparisons ($N = 8088$). The three plots on top are for (left to right) CLH and CSI, CLH and Harvard, and CSI and Harvard. The middle row plots are the same as those in the top row, except that they are \log_{10} IWC. Data are dots, the 1:1 line is dashed, and the linear best fit line is solid. In the bottom row of plots, the percent difference between the instruments is shown. Triangles and Xs are the median and mean of 2000 points, respectively, with the vertical line representing ± 1 standard deviation of the binned data.

CSI at small IWC also remain unexplained, although possible explanations include the known increases in uncertainty at low IWC or a particle sampling issue such as the rejection of particles below the cut size of the CVI or a systematic error in the CLH particle enhancement factor caused by bias in the particle size data [Davis *et al.*, 2007]. The stated nominal uncertainties for the three instruments are in the range of 10–20%, but for each the uncertainty increases with decreasing IWC to upwards of 50% at 1 mg m^{-3} . Seen in this light, the intercomparisons shown in Figures 1 and 2 seem reasonable, although the presence of large differences at low IWC is an area in need of improvement, given the

potential application of these instruments to measurements in thin cirrus.

3.2. Comparisons Versus Particle Size

[22] Incomplete ice particle evaporation is a potential issue for all three IWC instruments, due to the relatively short residence times within their heated inlets. Residence times during MidCiX for the CLH, CSI, and HT inlets are nominally 250 [Davis *et al.*, 2007], 85, and 160 ms [Weinstock *et al.*, 2006a], respectively. For the CSI, the volume flow rate through the instrument is fixed, so the residence time is a constant regardless of air speed or altitude. For CLH, the

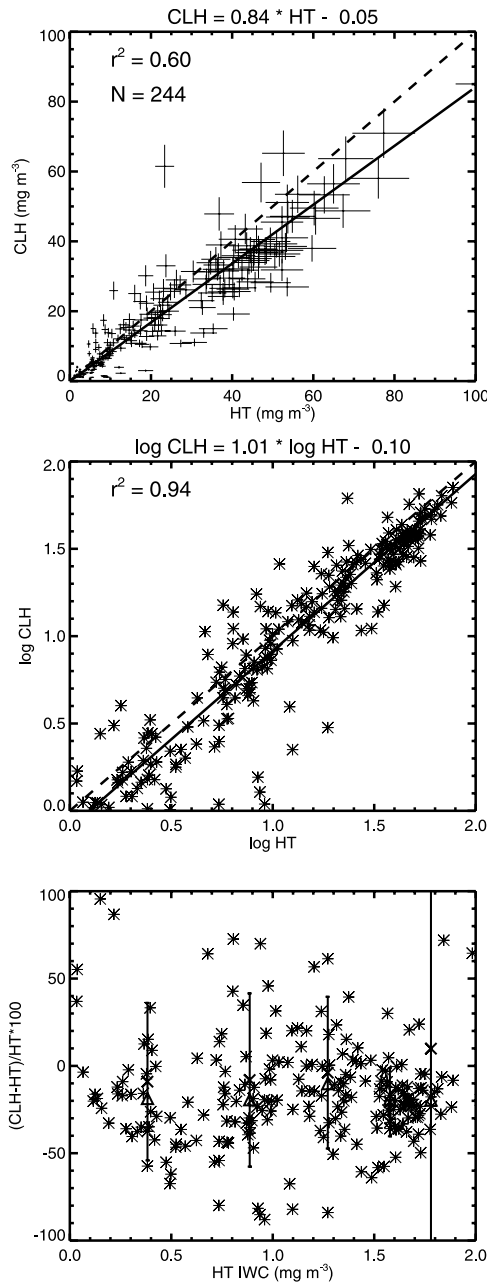


Figure 2. Comparison between CLH and HT ($N = 224$) IWC values for CRYSTAL-FACE. Plots in each row are similar to those in Figure 1, except that estimated error bars are shown in the top row and 20 measurements are averaged per bin in the bottom row.

mass flow rate through the instrument is set at a constant value for any given flight, so the residence time is a function of pressure only. Given the range of MFC set points during MidCiX and CRYSTAL-FACE (at $p < 400$ mb), the CLH residence times were ~ 120 – 410 ms (5th/95th percentile). Because the Harvard instrument maintains isokinetic flow, changes in airspeed affect the residence time. At altitudes relevant for cirrus measurements ($p < 400$ mb) during MidCiX and CRYSTAL-FACE, the WB-57 true air speed variations (~ 100 – 200 m/s) cause a range of residence times from 120 – 200 ms (5th/95th percentile) for Harvard. For

CLH and Harvard, when the residence time is smaller there is a greater likelihood that incomplete particle evaporation could be significant.

[23] To promote particle evaporation, the CSI and (post-CRYSTAL-FACE) HT inlets have stainless-steel mesh screens to break up particles before they enter the inlet. The CLH inlet contains three 90-degree bends so that particles larger than about $30 \mu\text{m}$ impact the wall at the first bend, shattering to smaller, more easily evaporated pieces.

[24] In general, estimating the maximum particle size evaporated is complicated due to incomplete knowledge of ice crystal geometry and density, size distributions of shattering by-products, and changes in the ambient relative humidity from evaporation within the inlets. Estimates of particle evaporation within the HT [Weinstock *et al.*, 2006a] and CLH [Davis *et al.*, 2007] inlets indicate that the maximum evaporated particle sizes are 150 and $30 \mu\text{m}$, respectively, in the absence of wall impacts. We note that the authors of these two articles use different analytical expressions for calculating particle evaporation, each of which makes different assumptions about the effects of ambient humidity, temperature gradient, etc.

[25] The issue of the extent of particle evaporation is investigated here using CAPS particle size distribution measurements from MidCiX and CRYSTAL-FACE. Figure 3 shows the percent difference in IWC between CLH, CSI, and HT as a function of several different proxies of particle size calculated from CAPS data. The left column shows the IWC differences as a function of the mean mass diameter, and the right column shows differences as a function of the fractional IWC at particle diameters greater than $150 \mu\text{m}$. The mean mass diameter is given by

$$D_{\text{mm}} = \frac{\sum_i N_i m_i D_i}{\sum_i N_i m_i} \quad (1)$$

with

$$m_i = \rho_{\text{ice}} \frac{\pi}{8} D_i^3 \quad (2)$$

where ρ_{ice} is the bulk density of ice (0.9 g cm^{-3}), D_i is the diameter of particles in the i th bin, m_i is the mass, and N_i is the particle concentration ($\# \text{ L}^{-1}$). Fractional IWC from particles with diameters greater than $150 \mu\text{m}$ is calculated similarly by dividing the mass in bins larger than $150 \mu\text{m}$ by the total mass. The CAPS data were processed and stored in terms of their area-equivalent diameter, so the mass-dimensional relationship for spherical particles in equation (2) is used. Alternative methods of calculating D_{mm} , including maximum-dimension-processed CAPS data with mass-dimensional relationships and fits to gamma distributions [Heymsfield *et al.*, 2004], give the same general trends as those shown in Figure 3. However, it should be noted that ice crystal shattering on inlets and aircraft surfaces, which would bias D_{mm} and fractional IWC $> 150 \mu\text{m}$ toward smaller values, is thought to be a significant problem for the CAPS (D. Baumgardner, personal communication, 2006). To date, no method exists by which to quantify and correct particle data for the effects of shattering. CPI data are not

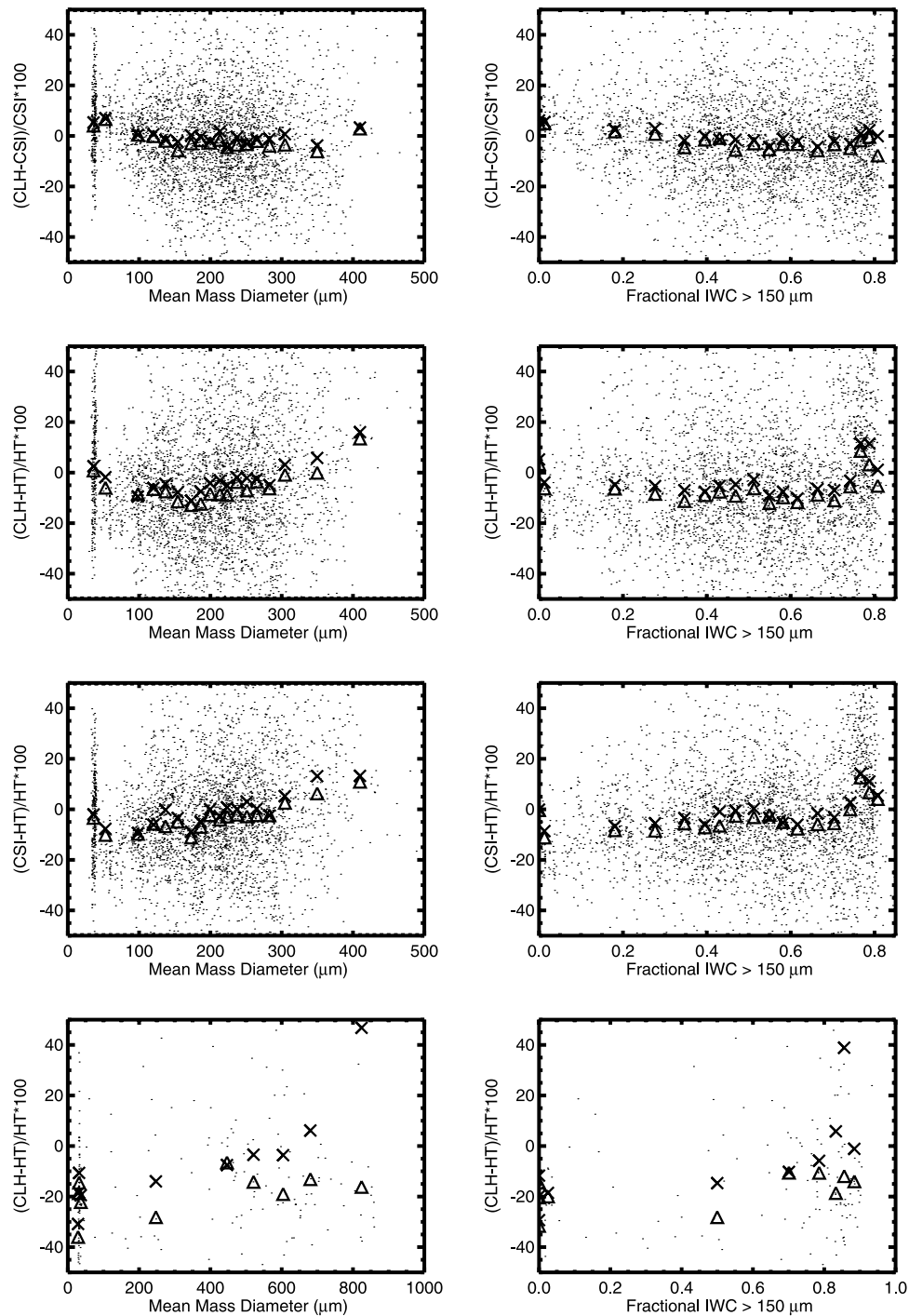


Figure 3. IWC percent differences versus mean mass diameter (left column) and fractional IWC at particle sizes greater than $150\ \mu\text{m}$, calculated from CAPS data for CRYSTAL-FACE (bottom row) and MidCiX (top three rows). Triangles and Xs are medians and means of 20 (CRYSTAL-FACE) or 200 (MidCiX) data points.

used in this comparison because the sample volume for large particles ($\sim 0.2\ \text{cm}^3$; Lawson *et al.*, 2001) is significantly smaller than that for the CIP portion of CAPS ($\sim 800\text{--}20,000\ \text{cm}^3$), and thus CPI may underestimate the concentrations of larger particles (A. Heymsfield, personal communication, 2006).

[26] Although slight trends are present in each comparison shown in Figure 3, they do not appear to explain the

general behavior of the comparisons in Figure 1. A slight increase of CSI and CLH relative to HT as a function of particle size is apparent in Figure 3. This is consistent with the possibility that large particles were not fully evaporated within the Harvard inlet, although the scattering signal in the HT data present during parts of CRYSTAL-FACE was greatly reduced or eliminated by the insertion of the stainless-steel screen before MidCiX. It seems unlikely that

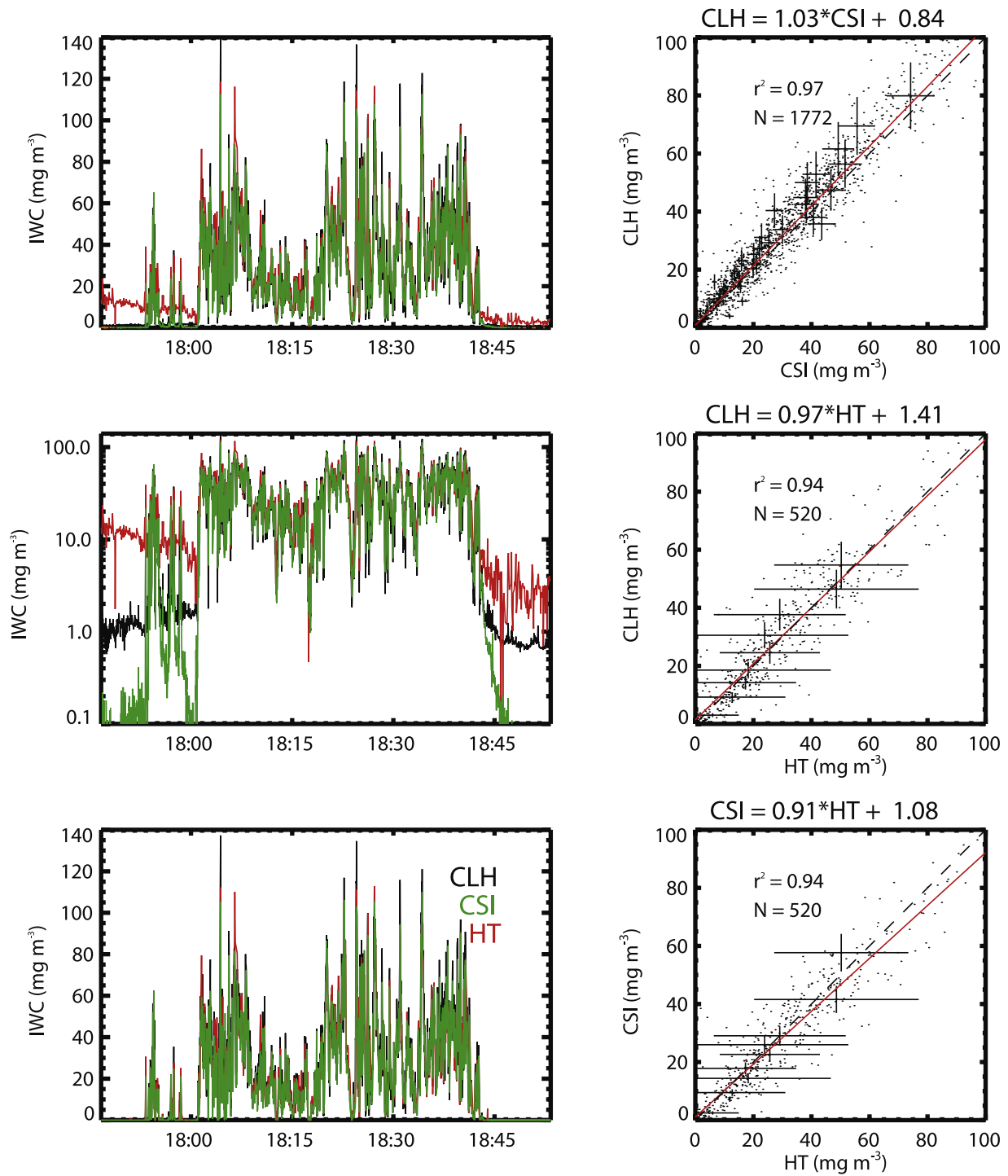


Figure 4. Left column, IWC from a 1-hour long cloud encounter over the Gulf of Mexico during the 2 May 2004 MidCiX flight, shown on both linear and log scales. The bottom plot shows the data with the clear-air backgrounds removed. Right column, IWC comparison plots for the same time period, with error bars plotted for every 50th data point.

incomplete evaporation is a significant contributing factor to these differences, but given the qualitative nature of the scattering signal, it cannot be ruled out completely.

[27] It is also unlikely, but impossible to rule out, that an unidentified particle sampling problem is causing the increase of CSI and CLH IWC relative to HT as a function of particle size. Although CSI and CLH both use subiso-

kinetic inlets, the designs are quite different, with significant differences in size-dependent sampling efficiencies. One would not expect the same errors in both and a lack of trend as shown in the top panel of Figure 3 would be unlikely if either instrument had an unidentified or unaccounted for sampling error. Also, for the particle sizes where these differences are seen, the CLH and CSI

sampling efficiencies are unity, and hence the IWC determinations are least sensitive to uncertainties in the particle size distribution. Although the precise cause of the trends seen in Figure 3 is unclear, Figure 3 should serve as an illustrative example that incomplete particle evaporation is not the major source of discrepancy among IWC measurements.

4. Cloud-Level Comparisons

4.1. Cirrus Associated With Upper-Level Trough: 2 May 2004 MidCiX Flight

[28] On 2 May 2004, a deep, midlatitude upper-level trough was positioned over east-central Texas and moist subtropical air was advecting in a northeasterly direction over the Gulf of Mexico, almost parallel to the Texas coast. The WB-57F flew through this air mass off the coast of Texas and sampled some of the densest cirrus encountered during the MidCiX mission, with IWC often larger than 100 mg m^{-3} . Figure 4 shows the ice water content as a function of time from the CLH, CSI, and HT instruments for a cloud encounter from approximately 17:47 to 18:53 UTC. The right column of Figure 4 shows the scatterplots of IWC for the instrument pairs during this time period, with the estimated instrumental uncertainties plotted as error bars for a few representative data points. The plots in Figure 4 show that the three instruments agree very well with one another, and appear to capture the same features on short temporal and spatial scales.

[29] Each instrument reports nonzero IWC in clear air, the presence of which is independently verified by the particle instruments and flight notes taken by the WB-57F on-board observer. The sources of nonzero clear-air IWC values are different for each instrument. For the CSI, backgrounds are related to sensor zero offset and, possibly, to water vapor entering the CVI. For the CLH, they are related to impurities (water vapor) in the nitrogen used for purging the laser and detector housings, as well as a detection threshold of about 10 ppm. For HT, backgrounds are likely caused by calibration drifts, due to deterioration in the optical properties of the vacuum ultraviolet (VUV) window for the lamp flux monitoring diode. Regardless of their cause, these background values are easily removed by calculating the constant clear-air offset between WV and eTW, and subtracting this value from the in-cloud IWC. Alternatively, one could multiplicatively scale the clear-air water vapor to match the eTW measurements, and then use the scaling to adjust the in-cloud values. This method is arguably more physically valid for Harvard (with the former more valid for the CLH and CSI), but the choice of scaling used here (additive) does not affect the results. In the end, the background values shown in this example are not a significant source of discrepancies between IWC values measured in cloud.

4.2. Mountain Wave Cloud Encounter: 5 May 2004 MidCiX Flight

[30] On 5 May 2004, the WB-57F aircraft targeted orographic cirrus over the Front Range of Colorado. Orographic cirrus clouds are characterized by low temperatures ($\sim -35^\circ\text{C}$) and relatively steady, low-turbulence airflow. In their interiors, homogeneous freezing of cloud droplets is thought to deplete the ambient relative humidity to the ice

saturation level [Heymsfield and Milosheovich, 1993, 1995]. The total water content (TWC) during the transit through the homogeneous freezing zone is approximately conserved, as the vapor excess above ice saturation is in the condensed phase.

[31] Future field campaigns with the WB-57F are likely to target thin tropical tropopause layer (TTL) cirrus, which are characterized by extremely low IWC ($\sim 0.1\text{--}1 \text{ mg m}^{-3}$), low water vapor ($\sim 10\text{--}50 \text{ ppm}$), and small ice crystals ($r_c \sim 10\text{--}25 \text{ }\mu\text{m}$) [McFarquhar et al., 2003; Sassen et al., 1989]. IWC measurements in orographic wave clouds present similar challenges to those anticipated in thin TTL cirrus. First, both thin TTL cirrus and orographic cirrus are thought to contain a relatively large number of small particles, which could be problematic for instruments such as the CSI and CLH that have size-dependent sampling characteristics. Of the three instruments, the CLH IWC is most sensitive to uncertainties in the particle size distribution. Also, if a significant contribution to IWC comes from particles below the cut size of the CSI, this would lead to a systematic underestimation of IWC by the CSI. Another measurement challenge that is similar between orographic cirrus and thin cirrus is the small contrast of the in-cloud (i.e., TW) signal relative to the out-of-cloud signal (water vapor). For the orographic cirrus encountered during the 5 May MidCiX flight, the water vapor density was roughly 20 mg m^{-3} , with the ice density on the order of 10 mg m^{-3} . Hence the contrast (TW/WV) was about 1.5 in this cloud encounter. For comparison, a thin TTL cirrus with IWC = 0.5 mg m^{-3} at 100 mb (water vapor $10 \text{ ppmv} = 1 \text{ mg m}^{-3}$) would also have a contrast of 1.5. All other things being equal (i.e., the percentage error in the TW/WV measurements being the same for these different clouds), the expected IWC error is the same. Finally, it should be noted that although there are similarities between wave clouds and thin TTL cirrus, the comparisons presented here may not be representative of the agreement in thin TTL cirrus because of instrument calibration and/or noise issues at the lower absolute WV and TW values.

[32] Figure 5 shows comparisons among the three IWC measurements in the orographic cirrus encounters from the 5 May 2004 flight. The plots in the left column show the IWC time series in three forms; linear, log, and linear with the out-of-cloud baselines removed. Comparisons of the in-cloud portion of the data (with out-of-cloud baselines removed) are shown in the right column of Figure 5, with 1σ -uncertainty estimates denoted by crosshairs. The sizes of the uncertainty estimates for HT ($\sim 50\%$) are primarily the result of the small contrast between total water and water vapor in these clouds. In contrast to prior comparisons, some of the data shown here lie outside of the 1σ -uncertainty estimates (especially in the CLH/CSI comparison). The fact that the out-of-cloud baseline values have been removed indicates that the differences cannot be explained by baseline offsets.

[33] The differences among the IWC values may be accounted for by one or some combination of several factors such as calibration problems at low IWC, mischaracterization of instrument uncertainty at low IWC, or particle sampling issues. The first two issues are difficult to account for, as the three instruments have never been simultaneously calibrated from the same system. However, all instruments

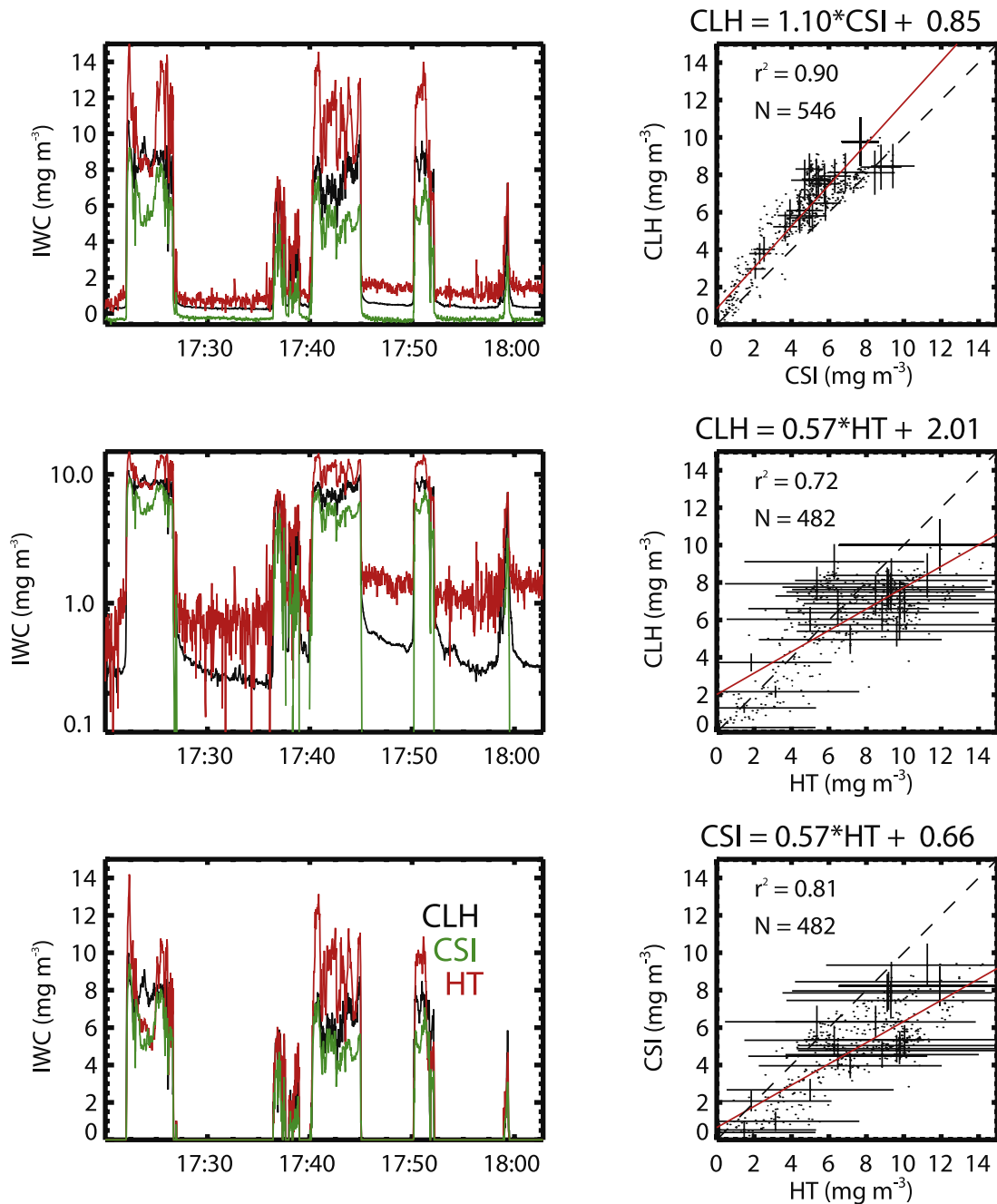


Figure 5. IWC comparisons, similar to Figure 4, for wave cloud encounters during the 5 May 2004 MidCiX flight. The upper two plots in the left-hand column are the IWC. The lower left-hand plot shows the data with the out-of-cloud baseline removed. These data are used for the comparisons in the right-hand column. Error bars show 1σ uncertainties in representative data points.

have been independently calibrated in the laboratory [Davis *et al.*, 2007; Heymsfield *et al.*, 2006; Weinstock *et al.*, 2006a].

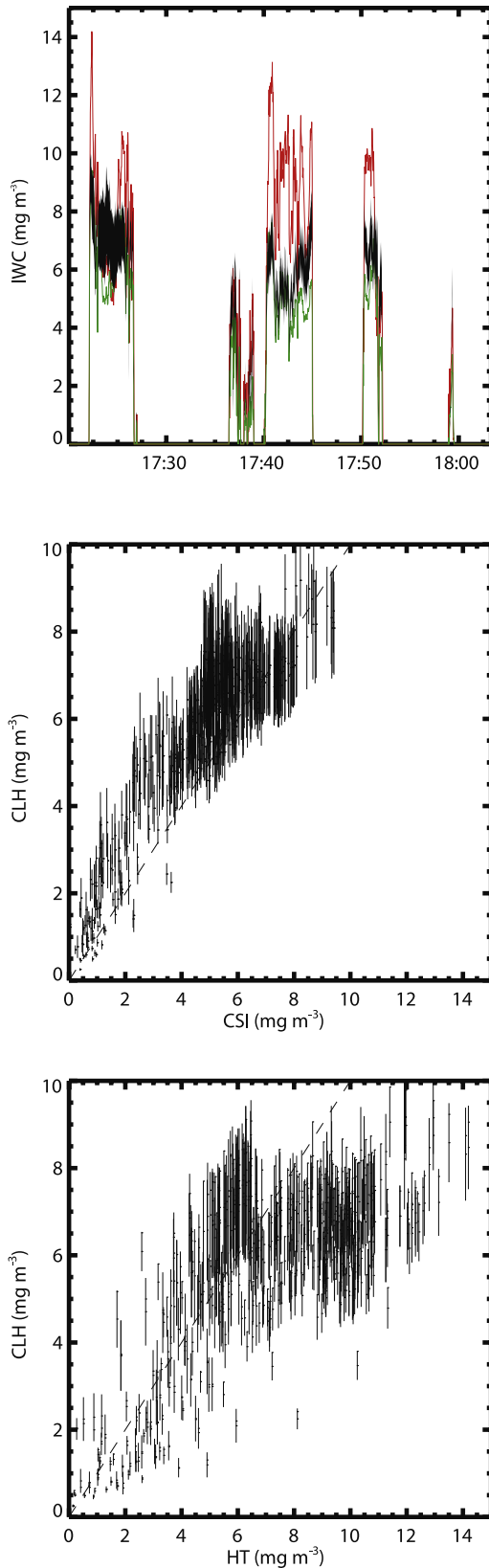
[34] Independent particle size data can be used to address the issue of whether or not differences in particle sampling among the instruments can explain the differing values of IWC observed during the 5 May flight. Each of the three instruments has different sampling characteristics, the salient features of which are mentioned in section 1 and described in detail in the cited papers. The CLH sampling efficiency ranges from 5% for $1\ \mu\text{m}$ diameter particles to

90% for $50\ \mu\text{m}$ particles, asymptoting to 100% for particles larger than $100\ \mu\text{m}$. In contrast, the HT has no size dependence, and the CSI sampling efficiency rises rapidly to 100% above the cut size of $\sim 5\ \mu\text{m}$. Although there is, in principle, a size dependence to the CSI sampling efficiency, it is unlikely that there is enough of a contribution to IWC from particles smaller than $5\ \mu\text{m}$ to significantly affect the IWC measurement. To address the issue of potential particle sampling differences, the sensitivity of the CLH IWC to assumptions about the particle size distribution is presented.

[35] The CLH IWC is given by $IWC = (eTW - WV)/X$, where eTW is the CLH-measured “enhanced” total water, WV is the ambient water vapor density, and X is the enhancement factor. Here we investigate the sensitivity of

CLH IWC to assumptions about particle size distributions by considering the range of values of X . The enhancement factor, X , is defined as $X = S(U/U_0)$, where S is the sampling efficiency (0–1), U is the aircraft true air speed, and U_0 is the instrument inlet speed. S is determined by integrating particle mass distributions with the CLH sampling efficiency curve [see *Davis et al.*, 2007 for details]. The quantity U/U_0 , which is commonly referred to as the inertial enhancement factor, is calculated from measured aircraft true air speed and instrument flow velocity.

[36] For the CLH IWC values shown thus far, the CLH enhancement factor was calculated for each data point using CAPS particle data. Calculating IWC using X determined from other particle data (CPI and FSSP) allows for an estimate of the upper bound on the IWC from effects of particle sampling, assuming the uncertainty in the CLH sampling efficiency curve is negligible. This curve was determined using a sophisticated three-dimensional computational fluid dynamics simulation [*Davis et al.*, 2007; *Engblom and Ross*, 2003] based on the actual geometry of the CLH inlet and the surrounding WB-57F structures (wingpod, fuselage, and wing). Calculating IWC using inertial enhancement factors (i.e., assuming $S = 1$) provides a lower bound for the CLH IWC by using the highest possible enhancement factor. The upper and lower bounds of CLH IWC calculated with four different values of S (CAPS, CPI, FSSP, and inertial enhancement) are shown in Figure 6, illustrating the sensitivity of the IWC determination to the various methods of computing X . While biases in the particle number concentration measurements (for example, undersampling of small particles related to sample volume uncertainties, overestimation of small particles resulting from particle shattering) are likely to exist, the data shown in Figure 6 indicate that particle sampling issues are unable to explain discrepancies between the CLH and CSI or HT observed during the 5 May MidCiX flight. Specifically, even though the CAPS number concentrations are about an order of magnitude higher than the FSSP’s during this time period, the RMS fractional difference between the CLH IWC calculated from FSSP and CAPS is 9% for the data shown in Figure 6.



5. Cloud Boundary Detection and Hysteresis

[37] The accurate detection of cloud boundaries is likely to be an important component of satellite validation activities with in situ measurements. Hysteresis, the presence of elevated water amounts related to desorption from instrument surfaces (or conversely reduced values from surface adsorption), has the potential to limit the ability of in situ measurements to detect cloud boundaries, as well as to introduce potential biases in IWC values. Previous efforts at

Figure 6. (Top plot) The CLH lower and upper IWC estimates (shaded black area), along with Harvard (red) and CSI (green). The lowest CLH IWC is determined using the inertial enhancement factor (U/U_0), while the upper line is the greatest of IWC determined from using FSSP, CAPS, or CPI particle size distributions. (Bottom two plots) Scatterplots of CLH versus CSI and CLH versus HT, with vertical lines representing the range of CLH estimates.

eliminating or minimizing the effects of hysteresis have included correcting individual cloud passes for hysteresis by adding back the postcloud signal [Gerber *et al.*, 1998], and simply excluding clouds with low water contents that might represent hysteresis [Heymisfield *et al.*, 2006].

[38] Hysteresis related to aircraft ascent (passage from regions of large water vapor to regions of smaller water vapor) and penetration of high-IWC cloud in the Harvard instrument has been explored using CRYSTAL-FACE data by Weinstock *et al.* [2006b]. This was found to contribute no more than $\pm 5\%$ uncertainty to the Harvard IWC measurement.

[39] Compared to Harvard, the CLH and CSI have mass flow rates roughly a factor of 50 slower and detection-region water vapor densities about a factor of 50 larger. Assuming multilayer adsorption of water vapor, larger detection-region water vapor values increase the mass of water on inlet walls. The slower flow rates mean that instrument dry-out occurs more slowly after passage through a cloud or wet air mass (for example, on ascent). In addition to flow rate and detection-region water vapor differences, there are several other factors that may affect hysteresis behavior in these instruments. First, the inlet materials and surface area-to-volume ratios are different in each instrument. Also, the enhancement factor must be taken into consideration when considering the effect on IWC determination of desorption (adsorption) of a given mass of water from (to) the instrument walls. That is, although the mass adsorbed/desorbed within the CLH and CSI is expected to be larger than that for HT, the water vapor amounts present at the detection region for a given IWC are also larger. Thus, potential biases in IWC may be similar, even though the hysteresis effect by mass is much higher in the CLH and CSI.

[40] In the following subsections, the imprecision in cloud boundary detection and the level of bias in the in-cloud IWC data resulting from hysteresis are estimated using signal trail-off after transit through cirrus clouds. The observed signal trail-off is presumed to be caused by the inlet walls drying out (net desorption) as dry, cloud-free air flows through the instruments. During MidCiX, opportunities to measure hysteresis were not ideal because of aircraft flight patterns and generally low contrast between TW and WV. However, the following examples illustrate that during MidCiX, hysteresis effects do not adversely affect the IWC, and are unable to account for discrepancies between the measurements.

5.1. Time Constants for Water Vapor Decay From IWC Instruments

[41] During the 2 May MidCiX flight, a relatively high IWC cloud was sampled for about 45 min, after which the aircraft flew through clear air for about 10 min before encountering another cloud (Figure 7). The cumulative water path during this time period was approximately 800 g m^{-2} . The Harvard, CLH, and CSI raw signals (i.e., CLH eTW, CSI eIWC, HT, HW) are shown in Figures 7a and 7b as the aircraft exits the cloud. IWC values from the particle instruments (CAPS and FSSP) were calculated by integrating the measured size distributions assuming spherical particle shape and a density of 0.9 g cm^{-3} , and are included in Figure 7c along with the bulk IWC values. Depending on which measure of IWC is used, the cloud

boundary occurs somewhere between about 18:43.30 and 18:45.15 UTC. This 105-s difference corresponds to a distance of almost 16 km.

[42] Using the trail-off in measurements at the end of the cloud, single exponential fits to the data yield time constants of 88, 86, and 71 s for the CLH, CSI, and HT, respectively (Figure 7d). For this analysis, the cloud boundary is set at 18:43.26 (vertical dotted line in Figure 7c), and the Harvard water vapor is subtracted from the CLH enhanced TW value to minimize differences that result from changes in water vapor caused by aircraft ascent that occurred after the end of the cloud. The calculated time constants are sensitive to the choice of end-of-cloud time because the small, cloud-related signal affects the curve fitting, but values in the 60–100 s range qualitatively fit the data reasonably well.

[43] One implication of the trail-off in signal at the end of cloud encounters is a resultant ambiguity in the location of cloud boundaries that is of the order of 10 km, given the aircraft speed. Also, these decay times represent timescales for sorption that are shorter than the duration of a typical cloud encounter, yet longer than the timescale for the (sub)second-scale IWC variations observed in cloud. Because of this, it is likely that a steady state condition is roughly approached, in which adsorption/desorption rates balance and the mass of water on the inlet walls is a function of the detection-region water vapor amount (averaged over the timescale for adsorption/desorption).

5.2. Estimating IWC Bias From Water Vapor Desorption

[44] A second method by which to assess hysteresis effects is to integrate the decay of water vapor after a cloud encounter to determine the mass of water desorbed from the instrument walls. Assuming a quasi-steady state is achieved within the instruments whereby the adsorption/desorption rates are roughly equal, the mass desorbed postcloud should be equal to the amount of mass stored on the instrument walls during the cloud transit. Such analysis cannot evaluate how quickly the mass is adsorbed to the inlet walls (and hence, how the IWC bias changes as a function of time within the cloud encounter), but can give an average IWC bias over the period of the cloud encounter.

[45] An example of this type of analysis is illustrated in Figure 7, which shows the decay of the raw signal and IWC values after a cloud encounter. To integrate the postcloud trail-off, the signals are shifted so that the mean value of each is zero over the last 50 data points. This is done so that the postcloud integration contains the decay of water vapor, independent of the background levels of each instrument. The area under each curve is then integrated and compared to the integrated in-cloud value.

[46] The above method was applied to five of the cloud encounters from MidCiX, including the two examples discussed in section 4. Figure 8 shows the percentage (ratio) of the postcloud to in-cloud mass, as a function of a scaled in-cloud mass (cloud mass divided by the smallest observed cloud mass). Although there were many more cloud encounters during MidCiX, those in this analysis were chosen because they were the most isolated in time from other clouds and did not contain periods of clear-air data within them. These criteria were chosen so that a distinct in-cloud and postcloud integration could be performed.

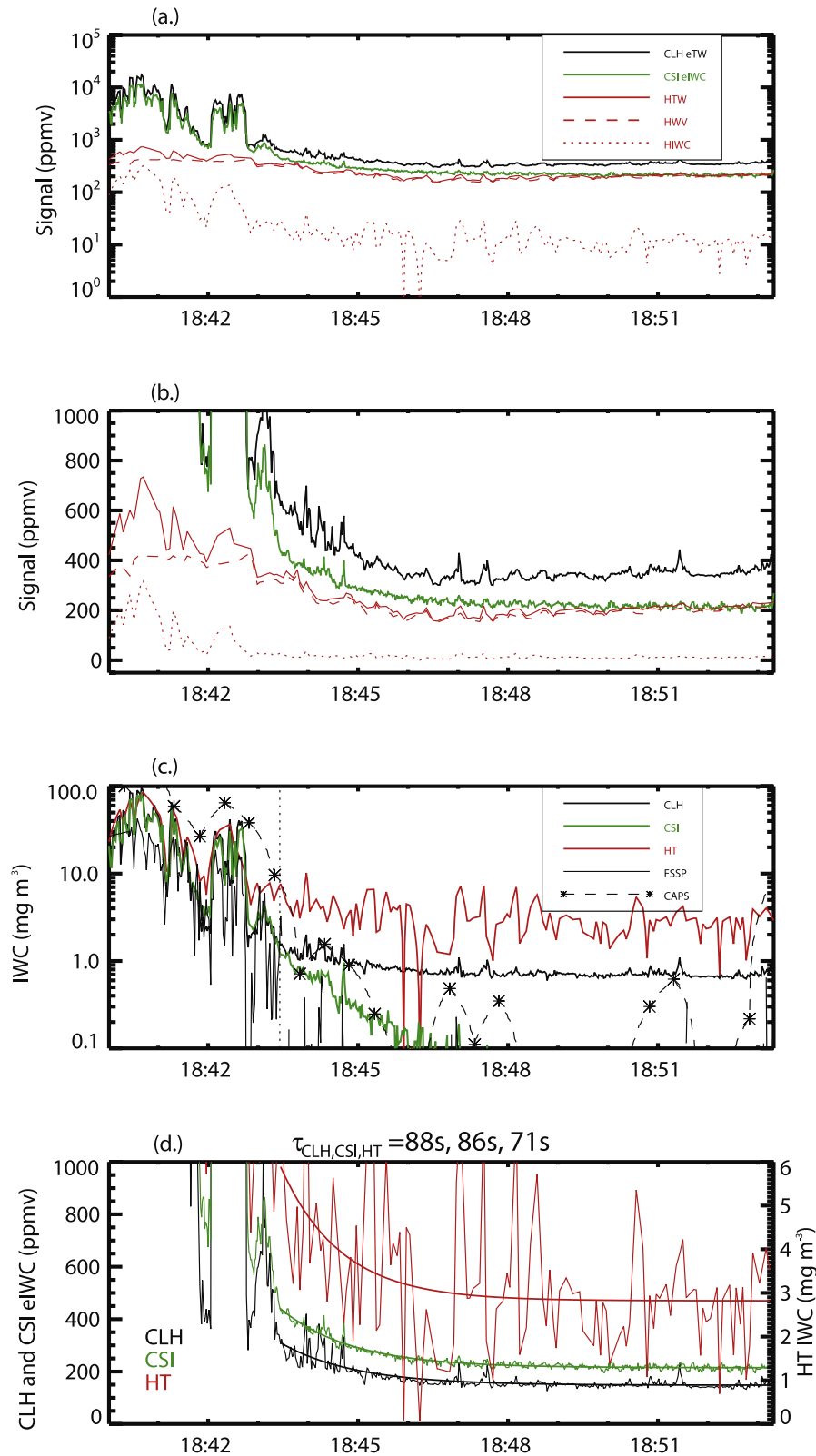


Figure 7. Instrument signal and IWC at the end of a cloud encounter on 2 May. The top two panels show the detection region water vapor amounts (i.e., CLH eTW, CSI eIWC, and HTW) that are used for determining IWC from the various instruments on (a) log and (b) linear scales. Figure 7c shows IWC from the CLH, CSI, and HT, as well as two of the particle instruments (CAPS and FSSP). The cloud boundary is somewhat ambiguous, but occurs between about 18:43.30 and 18:45.15. The cloud boundary assumed for subsequent analysis is marked by the vertical dotted line in Figure 7c. In Figure 7d, the postcloud signal trail-off is shown, along with the exponential fits to the data.

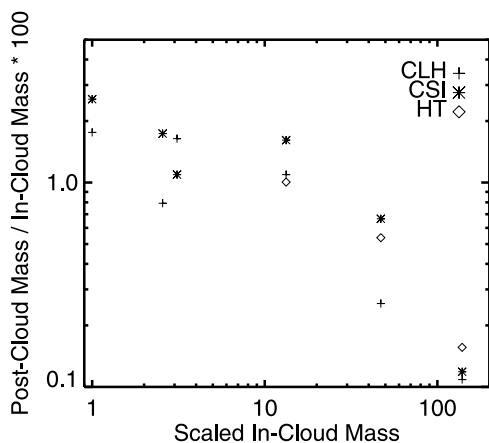


Figure 8. The percentage of postcloud desorbed mass to in-cloud mass, as a function of scaled in-cloud mass.

Nevertheless, some of the postcloud integrations for the Harvard instrument were not included in Figure 8 because there was no discernable trail-off in the signal. Figures 7a and 7b illustrate that the high (relative to IWC) and variable background water vapor typical of the MidCiX data set make it difficult, if not impossible, to detect a trail-off in the Harvard IWC data.

[47] The data in Figure 8 indicate that the percentage bias due to hysteresis is larger for small cloud paths and smaller for large cloud paths. This may seem counterintuitive in that one expects more mass to be adsorbed by the instruments when flying through more dense clouds, and this is likely the case. However, if adsorption and desorption rates approach steady state during a cloud encounter, the mass of water vapor stuck to instrument walls (i.e., the mass desorbed postcloud) is a fixed amount, and hence the larger the in-cloud mass, the smaller the ratio of the postcloud to in-cloud mass.

[48] Overall, the data in Figure 8 indicate that hysteresis effects on the IWC measurements during MidCiX are less than 3%, and thus do not present a significant source of uncertainty even in thin clouds. Finally, interpreting Figure 8 as a comparison between the hysteresis effects of the different instruments should be avoided. As can be seen in Figure 7, the noise level for each of the instruments is significantly different, and the postcloud integration is sensitive to both the noise level and the somewhat arbitrary definition of the end-of-cloud time. Rather, Figure 8 should be interpreted as a worst-case scenario, giving cause for concern only in clouds with the smallest of integrated masses such as those during the 5 May orographic cloud encounter. In these clouds, corrections using a model to quantify hysteresis may be needed [Gerber *et al.*, 1998; Weinstock *et al.*, 2006b], depending on the desired level of accuracy.

[49] Finally, it should be noted that hysteresis effects due to extremely large detection-region water vapor amounts (100,000 ppm or greater), in which there is potential condensation within the instruments, is not discussed here. CLH and CSI are prone to this type of effect because of particle enhancement, whereas HT is not. In these cases, some of which occurred with the CLH during

CRYSTAL-FACE, the data are considered invalid and not used for IWC determination.

6. Comparison of In Situ Ice Water Paths During MidCiX

[50] Most satellite retrievals of cloud properties are vertical-column-integrated values, whereas in situ measurements are observations of quantities at a point in space and time. Examples of vertically integrated quantities relevant to cirrus are optical depth and ice water path (IWP, g m^{-2}), with the corresponding in situ measurements being extinction and IWC. One potential application of in situ data from field campaigns such as MidCiX is for satellite validation.

[51] During MidCiX, the WB-57F flight patterns were coordinated with Terra and Aqua overpasses. The WB-57F performed Eulerian and Lagrangian spiral maneuvers during some of these overpasses, from which integrated quantities such as IWP can be calculated from the in situ IWC measurements. In this section, comparisons are made between IWPs calculated from the various IWC measurements, and the implications for satellite validation studies are addressed.

[52] An example vertical profile of IWC from the 27 April MidCiX flight is shown in Figure 9. During this flight, the WB-57F performed an 8-min-long upward Eulerian spiral maneuver. Figure 9 shows the vertical profile of IWC taken during this spiral from each of the instruments. The ice water paths calculated from this spiral are 77, 75, and 75 g m^{-2} for CLH, CSI, and HT, respectively.

[53] During MidCiX, there were 13 spiral maneuvers performed by the WB-57F. The targeted clouds ranged from thin cirrus associated with the subtropical jet to thicker convectively generated cirrus. Figure 10 shows three-way comparisons of the IWP calculated from the MidCiX spiral data set. Although the data set in Figure 10 is limited in size, the agreement between the various IWP values is within 20% for large IWP, and well within a factor of two for the thinnest cirrus. It is worth noting that the thinnest cirrus presented here had optical depths of about 0.1. The implication of this result is that, while there are inherent uncertainties in and disagreement among the IWC instruments, these shortcomings are unlikely to be limiting factors for

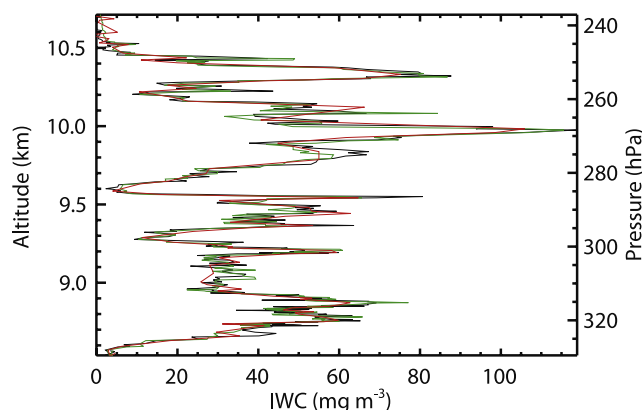


Figure 9. Vertical profile of IWC taken during a spiral maneuver on the 27 April MidCiX flight.

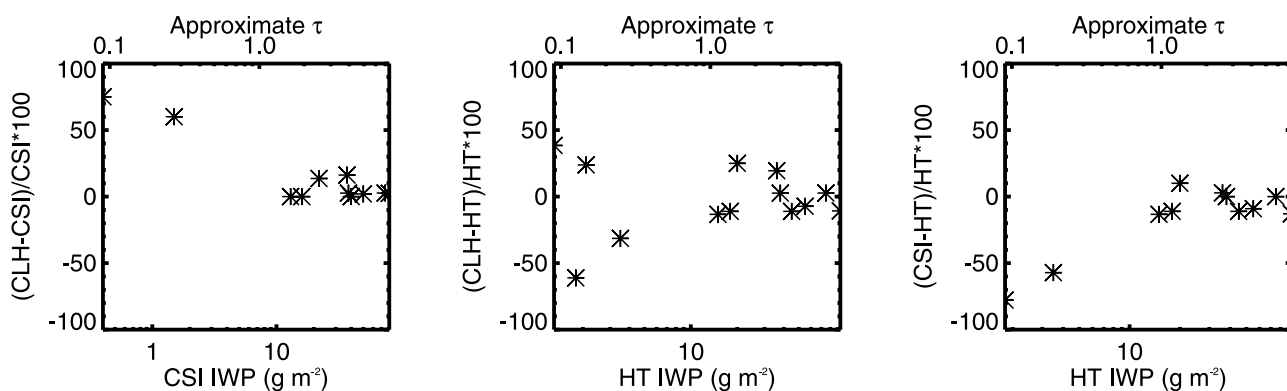


Figure 10. Comparisons of in situ IWPs calculated from the 13 Eulerian spiral maneuvers performed by the WB-57F during MidCiX.

satellite validation studies, except perhaps in the thinnest of cirrus. Although they have not been explored in detail, it is likely that other issues such as cloud inhomogeneities, collocation, and temporal evolution of the cloud field will present greater limitations to future satellite validation studies than instrument accuracy.

7. Summary

[54] Aircraft-based instruments that measure water vapor resulting from the evaporation of cloud ice crystals are expected to provide the fastest and most accurate determinations of cirrus cloud IWC available. The data generated by these instruments have been and will continue to be used in applications ranging from radiative transfer modeling to development of cirrus parameterizations for GCMs to validation of satellite and ground-based remote sensors. Because of the importance of these measurements, the inherent difficulty in measuring a variable over at least four orders of magnitude, and the lack of an absolute reference standard by which to judge instrumental accuracy, we have intercompared IWC measurements from the three “evaporative” instruments flown aboard the WB-57F aircraft to assess the extent of their agreement within the context of their estimated uncertainties.

[55] During the MidCiX campaign, the three instruments agree, on average, to within 20% of one another over a broad range of IWC values. At lower IWC amounts ($<10 \text{ mg m}^{-3}$), the agreement becomes worse, due in part to increasing instrument uncertainty at low contrast between (enhanced) TW and WV. This has implications for IWC measurements in very thin cirrus, where TW/WV contrasts are expected to be similar to or smaller than the lowest IWC cases from MidCiX. Possible causes of differences between the measurements such as baseline offsets, particle sampling, and adsorption/desorption-related hysteresis were addressed here, and are not found to be significant contributors to differences in observed IWC. However, because of uncertainties and potential biases in the particle probe data, the issue of particle sampling differences among the instruments should be further explored with future data sets. For satellite validation studies where the IWC data are vertically integrated to obtain IWP, the agreement between instruments is better than 20% for thick cirrus ($\tau > 1$), implying that IWC

measurements in thicker clouds are unlikely to be the limiting factor for satellite validation studies.

[56] In summary, the in situ measurements of cirrus IWC from three different instruments described here generally agree with one another within the bounds of their estimated uncertainties. This level of agreement lends confidence in the absolute accuracy of evaporation-based aircraft IWC measurements.

[57] **Acknowledgments.** Funding for participation in the CRYSTAL-FACE and MidCiX campaigns and subsequent data analysis described herein was provided to LMA, CT, EW, and JS by NASA’s Radiation Sciences Program, under the direction of Don Anderson and Hal Maring. SD recognizes the support of the NASA ESS Fellowship program, and numerous helpful discussions with Gannet Hallar, Andy Heymsfield, Darrel Baumgardner, and Paul Lawson. The authors appreciate the support and dedication of the WB-57F flight and ground crews.

References

- Aumann, H. H., et al. (2003), AIRS/AMSU/HSB on the Aqua mission: Design, science objectives, data products, and processing systems, *IEEE Trans. Geosci. Remote Sens.*, *41*, 253–264.
- Baumgardner, D., H. Jonsson, W. Dawson, D. O’Connor, and R. Newton (2001), The cloud, aerosol and precipitation spectrometer: A new instrument for cloud investigations, *Atmos. Res.*, *59–60*, 251–264.
- Davis, S. M., A. G. Hallar, L. M. Avallone, and W. E. Engblom (2007), Measurements of total water content with a tunable diode laser hygrometer: Inlet analysis, calibration procedure, and ice water content determination, *J. Atmos. Ocean. Technol.*, *24*, 3, 463–475.
- Engblom, W., and M. Ross (2003), Numerical Model of Airflow Induced Particle Enhancement for Instruments Carried by the WB-57F Aircraft, ATR-2004(5084)-1, El Segundo, CA.
- Gao, B. C., and Y. J. Kaufman (1995), Selection of the 1.375- μm MODIS channel for remote sensing of cirrus clouds and stratospheric aerosols from space, *J. Atmos. Sci.*, *52*, 4231–4237.
- Gerber, H., C. H. Twohy, B. Gandrud, A. J. Heymsfield, G. M. McFarquhar, P. J. DeMott, and D. C. Rogers (1998), Measurements of wave-cloud microphysical properties with two new aircraft probes, *Geophys. Res. Lett.*, *25*, 1117–1120.
- Hallar, A. G., L. M. Avallone, R. L. Herman, B. E. Anderson, and A. J. Heymsfield (2004), Measurements of ice water content in tropopause region arctic cirrus during the SAGE III Ozone Loss and Validation Experiment (SOLVE), *J. Geophys. Res.*, *109*, D17203, doi:10.1029/2003JD004348.
- Heymsfield, A. J., and L. M. Miloshevich (1993), Homogeneous ice nucleation and supercooled liquid water in orographic wave clouds, *J. Atmos. Sci.*, *50*, 2335–2353.
- Heymsfield, A. J., and L. M. Miloshevich (1995), Relative humidity and temperature influences on cirrus formation and evolution: Observations from wave clouds and FIRE II, *J. Atmos. Sci.*, *52*, 4302–4326.
- Heymsfield, A. J., A. Bansemmer, C. Schmitt, C. Twohy, and M. R. Poellot (2004), Effective ice particle densities derived from aircraft data, *J. Atmos. Sci.*, *61*, 982–1003.

- Heysmsfield, A. J., D. Winker, and G. J. van Zadelhoff (2005), Extinction-ice water content-effective radius algorithms for CALIPSO, *Geophys. Res. Lett.*, *32*, L10807, doi:10.1029/2005GL022742.
- Heysmsfield, A. J., C. Schmitt, A. Bansemmer, G. J. van Zadelhoff, M. R. J. McGill, C. Twohy, and D. Baumgardner (2006), Effective radius of ice cloud particle populations derived from aircraft probes, *J. Atmos. Ocean. Technol.*, *23*, 361–380.
- Houghton, J. T., and Intergovernmental Panel on Climate Change, Working Group I (2001), *Climate change 2001: The scientific basis: Contribution of Working Group I to the third assessment report of the Intergovernmental Panel on Climate Change*, x, 881 pp., Cambridge Univ. Press, New York.
- Jensen, E. J., D. Starr, and O. B. Toon (2004), Mission investigates tropical cirrus clouds, *Eos Trans. AGU*, *85*, 45–50.
- Joseph, E., and W. C. Wang (1999), An interactive cirrus cloud radiative parameterization for global climate models, *J. Geophys. Res.*, *104*, 9501–9515.
- Kao, C. Y. J., and W. S. Smith (1999), Sensitivity of a cloud parameterization package in the National Center for Atmospheric Research Community Climate Model, *J. Geophys. Res.*, *104*, 11,961–11,983.
- King, M. D., Y. J. Kaufman, W. P. Menzel, and D. Tanre (1992), Remote-sensing of cloud, aerosol, and water-vapor properties from the moderate resolution imaging spectrometer (MODIS), *IEEE Trans. Geosci. Remote Sens.*, *30*, 2–27.
- Lawson, R. P., and T. L. Jensen (1998), Improved microphysical observations in mixed clouds, paper presented at Conference on cloud physics, Am. Meteorol. Soc., Boston, Mass.
- Lawson, R. P., B. A. Baker, C. G. Schmitt, and T. L. Jensen (2001), An overview of microphysical properties of Arctic clouds observed in May and July 1998 during FIRE ACE, *J. Geophys. Res.*, *106*, 14,989–15,014.
- Li, J. L., et al. (2005), Comparisons of EOS MLS cloud ice measurements with ECMWF analyses and GCM simulations: Initial results, *Geophys. Res. Lett.*, *32*, L18710, doi:10.1029/2005GL023788.
- Liou, K. N. (1986), Influence of cirrus clouds on weather and climate processes—A global perspective, *Mon. Weather Rev.*, *114*, 1167–1199.
- Lohmann, U., and E. Roeckner (1995), Influence of cirrus cloud radiative forcing on climate and climate sensitivity in a general-circulation model, *J. Geophys. Res.*, *100*, 16,305–16,323.
- May, R. D. (1998), Open-path, near-infrared tunable diode laser spectrometer for atmospheric measurements of H₂O, *J. Geophys. Res.*, *103*, 19,161–19,172.
- McFarquhar, G. M., S. Iacobellis, and R. C. J. Somerville (2003), SCM simulations of tropical ice clouds using observationally based parameterizations of microphysics, *J. Clim.*, *16*, 1643–1664.
- Minnis, P., D. P. Kratz, J. A. Coakley Jr., M. D. King, D. Garber, P. Heck, S. Mayor, D. F. Young, and R. Arduini (1995), Cloud Optical Property Retrieval (Subsystem 4.3), in *Clouds and the Earth's Radiant Energy System (CERES) Algorithm Theoretical Basis Document*, vol. 3, *Cloud Analyses and Radiance Inversions (Subsystem 4)*, edited by CERES Science Team, pp. 135–176.
- Sassen, K., M. K. Griffin, and G. C. Dodd (1989), Optical-scattering and microphysical properties of subvisual cirrus clouds, and climatic implications, *J. Appl. Meteorol.*, *28*, 91–98.
- Scott, S. G., T. P. Bui, K. R. Chan, and S. W. Bowen (1990), The meteorological measurement system on the NASA ER-2 aircraft, *J. Atmos. Ocean. Technol.*, *7*, 525–540.
- Stephens, G. L., et al. (2002), The CloudSat mission and the A-train—A new dimension of space-based observations of clouds and precipitation, *Bull. Am. Meteorol. Soc.*, *83*, 1771–1790.
- Twohy, C. H., A. J. Schanot, and W. A. Cooper (1997), Measurement of condensed water content in liquid and ice clouds using an airborne counterflow virtual impactor, *J. Atmos. Ocean. Technol.*, *14*, 197–202.
- Vaughan, M. A., S. A. Young, D. M. Winker, K. A. Powell, A. H. Omar, Z. Liu, Y. Hu, and C. A. Hostetler (2004), Fully automated analysis of space-based lidar data: An overview of the CALIPSO retrieval algorithms and data products, paper presented at Laser Radar Techniques for Atmospheric Sensing, SPIE, Maspalomas, Gran Canaria, Spain.
- Waters, J. W., S. Fakeperson, and A. Fakeperson (2006), The earth observing system microwave limb sounder (eOS MLS) on the Aura satellite, *IEEE Trans. Geosci. Remote Sens.*, *44*, 1075–1092.
- Weinstock, E. M., E. J. Hints, A. E. Dessler, J. F. Oliver, N. L. Hazen, J. N. Demusz, N. T. Allen, L. B. Lapsen, and J. G. Anderson (1994), New fast-response photofragment fluorescence hygrometer for use on the NASA ER-2 and the Perseus remotely piloted aircraft, *Rev. Sci. Instrum.*, *65*, 3544–3554.
- Weinstock, E. M., et al. (2006a), Measurements of the total water content of cirrus clouds: Part I. Instrument details and calibration, *J. Atmos. Ocean. Technol.*, *23*, 1397–1409.
- Weinstock, E. M., J. B. Smith, D. Sayres, J. V. Pittman, N. Allen, and J. G. Anderson (2006b), Measurements of the total water content of cirrus clouds: Part II. Instrument performance and validation, *J. Atmos. Ocean. Technol.*, *23*, 1410–1421.

L. M. Avallone and S. M. Davis, University of Colorado, Laboratory for Atmospheric and Space Physics, 1234 Innovation Dr., Boulder, CO 80303, USA. (seand@colorado.edu)

G. L. Kok, Droplet Measurement Technologies, 5710B Flatirons Parkway, Boulder, CO 80301, USA.

J. B. Smith and E. M. Weinstock, Department of Chemistry and Chemical Biology, Harvard University, 12 Oxford St., Cambridge, MA 02138, USA.

C. H. Twohy, College of Oceanography and Atmospheric Sciences, Oregon State University, COAS Admin 104, Corvallis, OR 97331-5503, USA.